

# Geophysical Research Letters<sup>®</sup>



## RESEARCH LETTER

10.1029/2023GL104699

### Key Points:

- Lightning Mapping Array data reveals a positive correlation between lightning NO<sub>x</sub> production efficiency and the lightning flash lengths
- The investigation of space-based data demonstrates a negative correlation between lightning NO<sub>x</sub> production efficiency and flash frequency
- Mean NO<sub>x</sub> per flash length obtained in this work vary between  $1.9 \times 10^{21}$  and  $3.8 \times 10^{21}$  molec NO<sub>x</sub>/m

### Supporting Information:

Supporting Information may be found in the online version of this article.

### Correspondence to:

F. J. Pérez-Invernón,  
fjpi89@gmail.com

### Citation:

Pérez-Invernón, F. J., Gordillo-Vázquez, F. J., van der Velde, O., Montanyá, J., López Trujillo, J. A., Pineda, N., et al. (2023). Lightning-produced nitrogen oxides per flash length obtained by using TROPOMI observations and the Ebro Lightning Mapping Array. *Geophysical Research Letters*, 50, e2023GL104699. <https://doi.org/10.1029/2023GL104699>

Received 25 MAY 2023

Accepted 18 NOV 2023

### Author Contributions:

**Conceptualization:** Francisco J.

Gordillo-Vázquez, Oscar van der Velde, Joan Montanyá, Nicolau Pineda, Heidi Huntrieser

**Data curation:** Oscar van der Velde, Joan Montanyá, Jesús Alberto López Trujillo, Nicolau Pineda, Pieter Valks, Diego Loyola, Thilo Erbertseder










**Formal analysis:** Francisco J. Gordillo-Vázquez, Oscar van der Velde, Nicolau Pineda, Heidi Huntrieser, Pieter Valks

**Investigation:** Francisco J. Gordillo-Vázquez, Oscar van der Velde, Nicolau Pineda, Heidi Huntrieser

© 2023. The Authors.

This is an open access article under the terms of the [Creative Commons Attribution License](#), which permits use, distribution and reproduction in any medium, provided the original work is properly cited.

## Lightning-Produced Nitrogen Oxides Per Flash Length Obtained by Using TROPOMI Observations and the Ebro Lightning Mapping Array

Francisco J. Pérez-Invernón<sup>1</sup> , Francisco J. Gordillo-Vázquez<sup>1</sup>, Oscar van der Velde<sup>2</sup> , Joan Montanyá<sup>2</sup> , Jesús Alberto López Trujillo<sup>2</sup> , Nicolau Pineda<sup>2,3</sup> , Heidi Huntrieser<sup>4</sup> , Pieter Valks<sup>5</sup>, Diego Loyola<sup>5</sup> , Sora Seo<sup>5</sup> , and Thilo Erbertseder<sup>6</sup> 

<sup>1</sup>Instituto de Astrofísica de Andalucía (IAA), CSIC, Granada, Spain, <sup>2</sup>Lightning Research Group, Technical University of Catalonia, Terrassa, Spain, <sup>3</sup>Meteorological Service of Catalonia, Barcelona, Spain, <sup>4</sup>Deutsches Zentrum für Luft- und Raumfahrt, Institut für Physik der Atmosphäre, Wessling, Germany, <sup>5</sup>Deutsches Zentrum für Luft- und Raumfahrt, Methodik der Fernerkundung, Wessling, Germany, <sup>6</sup>Deutsches Zentrum für Luft- und Raumfahrt, Deutsches Fernerkundungsdatenzentrum, Wessling, Germany

**Abstract** Lightning is one of the main sources of NO<sub>x</sub> in the Earth's atmosphere. However, there is a large variability in NO<sub>x</sub> production during the lifetime of thunderstorms. In this study, we used the TROPospheric Monitoring Instrument (TROPOMI) cloud and NO<sub>2</sub> research products along with Lightning Mapping Array (LMA) measurements to investigate the possible relation between the amount of NO<sub>x</sub> produced per lightning flash and flash channel length in the Ebro Valley. We found that there is a positive relationship between both variables. In turn, the vertical structure of the analyzed lightning flashes indicates that longer flashes could release more LNO<sub>x</sub> at lower altitudes than shorter flashes, while higher flash rates produce less LNO<sub>x</sub> per flash.

**Plain Language Summary** Lightning produces significant amounts of NO<sub>x</sub> in the Earth's atmosphere. However, the quantity of NO<sub>x</sub> generated during thunderstorms exhibits significant variation. In this study, we used a space-based instrument called TROPOMI to look at clouds and measure NO<sub>2</sub>, and we also used a network of antennas called Lightning Mapping Array to map the spatial structure of lightning strikes. Our main goal was investigating if there is a connection between the amount of NO<sub>x</sub> produced by lightning and how long the lightning flashes were in the Ebro Valley. We found that there is a positive relationship between the two variables. We also looked at the structure of the lightning flashes and found that longer flashes release more NO<sub>x</sub> at lower altitudes compared to shorter flashes. Additionally, when there are more frequent lightning flashes, each flash produces less NO<sub>x</sub>.

## 1. Introduction

Hot plasma in lightning channels causes dissociation of air molecules into atomic nitrogen and oxygen. The fast cooling of the plasma contributes to the formation of nitrogen oxides (NO<sub>x</sub> = NO + NO<sub>2</sub>) by the Zeldovich mechanism (Zeldovich et al., 1947). The NO<sub>x</sub> produced by lightning (LNO<sub>x</sub>) in the troposphere plays a significant role in the budget of tropospheric ozone and in the oxidizing capacity of the atmosphere (Gordillo-Vázquez et al., 2019). Lightning contributes about 10% to global NO<sub>x</sub> emissions and up to nearly 20% in the tropics (Schumann & Huntrieser, 2007, and references therein), producing between 2 and 8 Tg N per year globally, which corresponds to 100–400 mol NO<sub>x</sub> per flash. Despite significant advances achieved by aircraft campaigns, laboratory measurements and by the improvement of satellites observations during the last decades, reducing the uncertainty in the production of NO<sub>x</sub> by lightning and understanding its variability is still a challenge.

The retrieval of NO<sub>2</sub> by nadir-viewing satellites, such as the Ozone Monitoring Instrument (OMI), the Scanning Imaging Absorption spectrometer for Atmospheric CHartographY (SCIAMACHY), and the Sentinel-5P TROPospheric Monitoring Instrument (TROPOMI), have provided an unprecedented opportunity to systematic LNO<sub>x</sub> Production Efficiency (PE) estimates over different regions (Allen et al., 2019; Allen, Pickering, Bucsela, et al., 2021; Bucsela et al., 2019; Pickering et al., 2016). Recent LNO<sub>x</sub> estimates based on satellite instruments suggest that the LNO<sub>x</sub> PE per flash falls at the lower end of the range of estimations reported in literature (100–400 mol NO<sub>x</sub> per flash) (Beirle et al., 2004; Schumann & Huntrieser, 2007). In particular, LNO<sub>x</sub> estimates based on TROPOMI NO<sub>2</sub> retrieval, the most modern global air quality satellite in operation, have produced LNO<sub>x</sub>

**Methodology:** Francisco J. Gordillo-Vázquez, Oscar van der Velde, Nicolau Pineda, Heidi Huntrieser, Diego Loyola

**Software:** Oscar van der Velde, Jesús Alberto López Trujillo, Pieter Valks, Diego Loyola, Thilo Erbertseder

**Supervision:** Francisco J. Gordillo-Vázquez

**Validation:** Oscar van der Velde, Joan Montanyà, Nicolau Pineda, Heidi Huntrieser, Pieter Valks, Diego Loyola, Thilo Erbertseder

**Visualization:** Pieter Valks, Diego Loyola, Thilo Erbertseder

**Writing – review & editing:** Francisco J. Gordillo-Vázquez, Oscar van der Velde, Nicolau Pineda, Heidi Huntrieser, Pieter Valks, Diego Loyola, Thilo Erbertseder

PE estimates of  $175 \pm 100$  mol and  $120 \pm 65$  mol  $\text{NO}_x$  per flash in the United States of America (USA) (Allen, Pickering, Bucselá, et al., 2021) by using lightning measurements from the Geostationary Lightning Mapper (GLM) and the Earth Networks Global Lightning Network (ENGLN), respectively,  $58 \pm 44$  mol  $\text{NO}_x$  per flash in the Ebro Valley and the Pyrenees (Pérez-Invernón et al., 2022), and  $60 \pm 33$  mol  $\text{NO}_x$  per flash in southeastern China (Zhang et al., 2022).

Some studies based on laboratory discharges have reported a positive relationship between the flash energy and the production of  $\text{LNO}_x$  (Allen, Pickering, Lamsal, et al., 2021; Schumann & Huntrieser, 2007; Stark et al., 1996; Wang et al., 1998). According to literature estimates, the production of  $\text{NO}_x$  per discharge energy ranges between  $1.4 \times 10^{16}$  and  $30 \times 10^{16}$  molecules  $\text{J}^{-1}$  (Schumann & Huntrieser, 2007). Several studies using satellite retrieval of  $\text{NO}_2$  have found an inverse relationship between flash rates and  $\text{LNO}_x$  PE per flash (Allen et al., 2019; Allen, Pickering, Bucselá, et al., 2021; Bucselá et al., 2019), while airborne studies suggest that there is a proportional relationship between flash length and  $\text{LNO}_x$  PE per flash (Huntrieser et al., 2007, 2008; Schumann & Huntrieser, 2007; Stith et al., 1999; Wang et al., 1998) ranging between  $0.5 \times 10^{21}$  and  $10 \times 10^{21}$  molecules  $\text{NO}_x \text{ m}^{-1}$ . The reported inverse relationship between flash rates and flash size (Bruning & MacGorman, 2013) explains the observed correlation between flash rates and  $\text{LNO}_x$ . Rahman et al. (2007) reported the first lightning measurements of  $\text{LNO}_x$  produced by rocket-triggered lightning. They found a production of  $2.0 \times 10^{22}$ – $2.4 \times 10^{22}$  molecules  $\text{NO}_x \text{ m}^{-1}$ . Finally, Mecikalski and Carey (2018) reported that the total length and the vertical structure of lightning flashes can influence the production of  $\text{LNO}_x$  by using two dimensional (2-D) histogram distributions of lightning flashes.

Very High Frequency (VHF) Lightning Mapping Arrays (LMAs) can locate the origin and propagation path of lightning channels within the cloud at high spatial and temporal resolution. In turn, LMA measurements can be used to calculate flash channel lengths for  $\text{LNO}_x$  estimates. In this context, Hansen et al. (2010) proposed to use LMA measurements to investigate the vertical distribution of  $\text{LNO}_x$ . The NASA Lightning Nitrogen Oxides Model (LNOM) uses LMA data from the North Alabama LMA (NALMA) (Koshak et al., 2014) and the laboratory results of Wang et al. (1998) to parameterize the production of  $\text{NO}_x$  per flash length in air quality models. More recently, Bruning and Thomas (2015) developed several models to estimate flash lengths from LMA measurements and discussed the sensitivity of  $\text{LNO}_x$  estimates to flash channel lengths.

In this work, we investigate the relationship between  $\text{LNO}_x$ , lightning flash length and lightning flash rate. We used the Deutsches Zentrum für Luft- und Raumfahrt (DLR) TROPOMI operational cloud and TROPOMI research  $\text{NO}_2$  products, also known as TROP-DLR (Liu et al., 2021; Loyola et al., 2018; Pérez-Invernón et al., 2022), combined with lightning measurements from the Ebro LMA (ELMA) (López et al., 2017; Pineda et al., 2016; van der Velde & Montanyà, 2013) and from the ENGLN (Lapierre et al., 2020; Zhu et al., 2017) for 16 cases. The ELMA system covers the Ebro Valley and the eastern coast of the Iberian Peninsula, an area with a high occurrence of thunderstorms during the end of the summer. During the end of the summer, the Mediterranean sea is warm and humid, favoring the development of thunderstorms when westerly frontal systems are passing by Pineda et al. (2010). Thunderstorms produced at the end of the summer by this mechanism have particular high updrafts and high lightning activity, although winter thunderstorms with high lightning activity in this region are not rare.

## 2. Data Sets and Methods

In this section, we describe the data sets and the methods used to investigate the relationships between  $\text{LNO}_x$  per flash, flash rates and flash lengths in the Ebro Valley.

### 2.1. TROP-DLR Operational and Research Products

The TROPOMI instrument started its operation on 13 October 2017 from a low Earth polar orbit on board the European Space Agency Sentinel-5 Precursor satellite. TROPOMI is a passive imaging spectrometer with eight spectral bands that provide daily global measurements of cloud properties and several trace gases (Veefkind et al., 2012). Among others, the final TROPOMI product includes the Slant Column Density (SCD) of  $\text{NO}_2$ , the error of the SCD  $\text{NO}_2$ , the quality assurance (QA) value, the stratospheric Vertical Column Density (VCD) of  $\text{NO}_2$ , the stratospheric Air Mass Factor (AMF) of  $\text{NO}_2$ , the Cloud Fraction (CF), Cloud Optical Thickness (COT), and the Optical Centroid Pressure (OCP) with a  $3.5 \text{ km} \times 7.0 \text{ km}$  horizontal resolution at nadir before 6 August 2019 and  $3.5 \text{ km} \times 5.5 \text{ km}$  thereafter.

In this work, we used the TROP-DLR operational cloud and NO<sub>2</sub> research products (Liu et al., 2021; Loyola et al., 2018), that were recently applied by Pérez-Invernón et al. (2022) for LNO<sub>x</sub> PE estimates. The TROP-DLR NO<sub>2</sub> research product is more appropriate for estimating LNO<sub>x</sub> than the operational TROPOMI NO<sub>2</sub> product because it produces more reliable cloud properties and NO<sub>2</sub> estimates over bright areas, such as thunderclouds. The cloud properties are derived by the OCRA/ROCINN algorithms by using the Clouds-As-Layers (CAL) model (Loyola et al., 2018). Clouds are treated as optically uniform layers using a more realistic cloud scattering model than the Cloud as Reflecting Boundaries (CRB) model implemented in the operational TROPOMI NO<sub>2</sub> product (Van Geffen et al., 2022). In turn, the TROP-DLR NO<sub>2</sub> research product uses a Directionally dependent STRatospheric Estimation Algorithm from Mainz (DSTREAM) to separate the contribution of the troposphere and stratosphere to the NO<sub>2</sub> column density (Liu et al., 2021) without requiring any input from atmospheric models. Following Pérez-Invernón et al. (2022), we used TROPOMI pixels with a SCD NO<sub>2</sub> error less than  $2 \times 10^{19}$  molec m<sup>-2</sup>. In turn, we define pixels with deep convection as those with an effective cloud fraction greater than 0.95 and an OCP less than 534 hPa. We obtain 20,637 pixels with deep convection and a SCD NO<sub>2</sub> error lower than  $2 \times 10^{19}$  molec m<sup>-2</sup>. In turn, we get 51 pixels with deep convection and a SCD NO<sub>2</sub> error above than  $2 \times 10^{19}$  molec m<sup>-2</sup>. The total number of pixels with deep convection for each case are presented in Table S1 in Supporting Information S1.

## 2.2. Lightning Measurements

ELMA is a VHF time-of-arrival network (Rison et al., 1999) consisting of 7 VHF receiver stations during the period of study (2018–2020). Table S1 in Supporting Information S1 shows the total number of active ELMA stations (5–7) for each case. Lightning sources are located using a minimum of 5 stations. The quality of data is a function of the number of active stations, the distance of the lightning activity, the background noise threshold at each station and the lightning direction with regard to the geometry of the network. ELMA produces the 3-dimensional locations of VHF sources in time. These are first processed by a simple filter to remove scattered sources (less than 3 in a grid cell of  $3 \times 3 \times 1$  km every 75 ms). Then, the sources are grouped into flashes by a source interval criterion of <75 ms. These “first guess” flashes may consist of multiple flashes occurring simultaneously in different thunderstorm cells. A second pass identifies flashes from just one or more contiguous clusters of 4 km grid cells. If there are separate groups, the corresponding sources are assigned to separate flashes. This usually works well unless a new flash starts at the same location as the previous flash before that one ended all leader extension, in which case the new and old flash are counted as one. This, however, occurs rarely in the storms in this geographic region. Another exception occurs when the system fails to detect all continuous leader activity of a flash, usually those at large distance from the LMA center. We choose 75 ms without sources as the criterion used to chop bursts of sources into subsequent flashes. In case the continuous leader activity in a flash (e.g., van der Velde and Montanyà (2013)) is not detected well, usually far from the LMA, the flash would be split up into two (or more) separate flashes.

We calculated the maximum length following the box counting method (number of boxes times their size) shown in Figure 3a of Bruning and Thomas (2015). This is the flash length calculated at the finest scale the LMA is capable of resolving. We performed this method for layers 2 km in depth, overlapping by 1 km. The total flash volume is calculated by summing the flash length across the depth of the thunderstorm. The result is a measure of flash volume that is not as sensitive to data quality as a fixed fine grid would be, as it adapts to decreasing resolution at larger distances from the network center. The total number of active ELMA stations for each case is shown in Table S2 in Supporting Information S1. It is important to mention that the calculation of the flash channel length is independent from the calculation of the LNO<sub>x</sub>.

As the Detection Efficiency (DE) of ELMA decays with the distance to the cluster of sensors, we used lightning measurements from ENGLN to obtain the total lightning in the area and calculate the total LNO<sub>x</sub> per flash. Then, we compared the median and the mean flash channel length with the total LNO<sub>x</sub> per flash for each case. For the calculation of the total LNO<sub>x</sub> per flash, we took into account that the total DE of ENGLN over the Ebro Valley is about 68% (Pérez-Invernón et al., 2022). We refer to Pérez-Invernón et al. (2022) for further details on the characteristics of lightning measurements provided by ENGLN in the Ebro Valley. One limitation that can result from the inhomogeneity in the DE of ELMA is that it detects fewer sources as lightning events occur at greater distances from the sensors, thus influencing the calculation of flash length. This is an inherent limitation in the use of LMA, and since there is no other source of information available on flash length, its effect is challenging

to quantify. That's why we focus on a significant number of cases with high lightning activity in the Ebro Valley, where the DE of ELMA is higher.

### 2.3. LNO<sub>x</sub> PE Estimate

We calculated the LNO<sub>x</sub> PE per flash for 16 cases by using the TROPOMI LNO<sub>x</sub> PE method proposed by Allen, Pickering, Bucselá, et al. (2021) and later employed by Pérez-Invernón et al. (2022). We limited the studied area to the region within the coverage of ELMA (38.4–42.5N latitude and 1.2W–3E longitude). We used the same simulation from the ECMWF–Hamburg (ECHAM)/Modular Earth Submodel System (MESSy version 2.54.0) Atmospheric Chemistry (EMAC) model (Jöckel et al., 2016) performed by Pérez-Invernón et al. (2022) to extract the mean LNO<sub>2</sub> and LNO<sub>x</sub> profiles that are needed to derive the air mass factors (AMFLNO<sub>x</sub>) used to estimate the vertical column density of LNO<sub>x</sub> from the slant column density of NO<sub>2</sub> provided in the TROP-DLR research product over pixels with deep convection. We define the deep convective constraint as TROPOMI pixels with a cloud fraction greater than 0.95 and OCP value less than 534 hPa. Following Pérez-Invernón et al. (2022), we included in the calculation of LNO<sub>x</sub> PE only flashes that are reported by ENGLN up to 5 hr prior to the TROPOMI overpass of each pixel. The lifetime of NO<sub>x</sub> in the near field of convection can range between 2 hr and 2 days (Nault et al., 2017; Pickering et al., 2016). In this work, we assumed that the lifetime of NO<sub>x</sub> in the near field of convection is 5 hr, which is a consensus value in LNO<sub>x</sub> estimates (Allen, Pickering, Bucselá, et al., 2021; Pérez-Invernón et al., 2022).

We estimated the background-NO<sub>x</sub> (not produced by lightning) in the troposphere as the 30th and the 10th percentiles of the Vertical Column Density (VCD) tropospheric NO<sub>x</sub> over non-flashing pixels (pixels where there are not reported lightning flashes) satisfying the deep convective constraint that are not affected by the advected LNO<sub>x</sub>. We used the wind velocity and direction averaged between 200 hPa and 500 hPa provided by the European Center for Medium-Range Weather Forecasts (ECMWF) ERA5-reanalysis data set (Hersbach et al., 2020) to estimate the pixels that are influenced by the advected LNO<sub>x</sub> Pérez-Invernón et al. (2022). The zonal component of the averaged wind is obtained by averaging the zonal component of the wind at all vertical points between the pressure levels 200 hPa and 500 hPa. Similarly, the meridional component of the wind is obtained by averaging the meridional component between these levels. The module of the averaged wind velocity and the averaged direction are shown in Figure S33 in Supporting Information S1. This method for determining the pixels that may not have been affected by the advected LNO<sub>x</sub> is a rough but valid approach for our purposes. It is a conservative criterion to reliably identify which pixels have not been affected by the LNO<sub>x</sub>.

## 3. Results and Discussion

### 3.1. Selected Case Studies

The eastern coast of the Iberian Peninsula comprises several large cities and agricultural areas where high anthropogenic emissions of NO<sub>x</sub> are located (Petetin et al., 2023). Therefore, we only included in our analysis thunderstorms producing a considerable high amount of fresh-produced LNO<sub>x</sub> to ensure that the LNO<sub>x</sub> signal is detectable. For this purpose, we only select cases with more than 1,000 lightning flashes 5 hr before the TROPOMI overpass or, alternatively, with more than 250 flashes during 1 hr before the TROPOMI overpass. The 16 selected cases can be found in the first column of Table S1 in Supporting Information S1 and corresponded to cases with active thunderstorms within the ELMA coverage. The second column of Table S1 in Supporting Information S1 lists the total number of active ELMA stations for each case.

The upper left panel of Figures S1–S16 in Supporting Information S1 show the SCD NO<sub>2</sub> data provided by the TROP-DLR research NO<sub>2</sub> product. The upper right panel depicts the flashes reported by ENGLN up to 5 hr before the TROPOMI overpass and the calculated VCD NO<sub>x</sub> over pixels with deep convection satisfying the quality constraint (SCD NO<sub>2</sub> error lower than  $2 \times 10^{19}$  molec m<sup>-2</sup>) after subtracting the background (10th percentiles of the Vertical Column Density (VCD) tropospheric NO<sub>x</sub> over non-flashing pixels) for the 16 studied cases. In the 16 cases, a significant total number of pixels have positive values of VCD NO<sub>x</sub> in the vicinity of lightning flashes. In particular, we obtain 15,240 pixels 5,367 and pixels with positive and negative values of VCD NO<sub>x</sub>, respectively. The total number of pixels with positive and negative values of VCD NO<sub>x</sub> for each case can be seen in Table S1 in Supporting Information S1. In Figures S6–S8, S10, S11, S13, and S14 in Supporting Information S1, VCD NO<sub>x</sub> and the lightning flashes are displaced to each other by a certain distance. This is



a consequence of the wind advecting  $\text{NO}_x$  and the existence of non-flashing deep convective pixels that will be used to estimate the background- $\text{NO}_x$ . These panels reveal that, in general, areas with lightning activity and also areas in the vicinity of large cities have higher SCD  $\text{NO}_2$  values. This correlation between lightning flashes and SCD  $\text{NO}_2$  values allows for the distinction between  $\text{LNO}_x$  signals and anthropogenic emissions, with two notable exceptions observed on 12 August 2018 and 23 August 2018 (see Figures S2 and S4 in Supporting Information S1, respectively). During those days, the TROPOMI overpass coincided with the formation of a thundercloud that had developed within the hour before. The OCP value was low, indicating high cloud tops that potentially resulted in a reduction of observed SCD  $\text{NO}_2$  values due to the greater amount of troposphere present below the clouds. The reported association between high lightning activity and low OCP values are in agreement with Bucselá et al. (2019). Finally, the lower right and left panels of Figures S1–S16 in Supporting Information S1 show the cloud fraction and the OCP provided by the TROP-DLR operational cloud product, respectively. Lightning flashes take place in pixels with a high cloud fraction and a low OCP value, as expected. Figures S17–S32 in Supporting Information S1 show the flashes detected by ELMA that are used to estimate the flash channel lengths. In general, there is a good agreement between spatial distribution of the flashes detected by ENGLN (second panel of Figures S1–S16 in Supporting Information S1) and by ELMA (Figures S17–S32 in Supporting Information S1). However, some cases exhibit remarkable differences because the DE of ELMA depends on the distance to the sensors. Despite differences in some cases, it is important to note that ELMA data is only used to estimate the length of flashes in the studied cases, while ENGLN is used to calculate  $\text{LNO}_x$  per flash.

Table S3 shows the total number of flashes reported by ENGLN and the relevant parameters derived from the TROP-DLR products. The total number of flashes reported by ENGLN for these thunderstorms ranged between 650 on 23 August 2018 and 39,452 on 17 August 2018. The mean values are 456 hPa for OCP, 1.9 hr for flash age,  $0.9 \times 10^{19}$  molec  $\text{m}^{-2}$  for  $V_{\text{tropNO}_x}$ ,  $8.0 \times 10^{19}$  molec  $\text{m}^{-2}$  for  $V_{\text{stratNO}_2}$ , 0.63 for  $\text{AMF}_{\text{LNO}_x}$ , and  $-0.33 \times 10^{19}$  molec  $\text{m}^{-2}$  and  $0.20 \times 10^{19}$  molec  $\text{m}^{-2}$  for  $V_{\text{tropbck}}$  when using the 10th and the 30th percentiles of the VCD tropospheric  $\text{NO}_x$  over non-flashing pixels satisfying the deep convective constraint, respectively. The values presented in Table S3 in Supporting Information S1 are comparable to the values derived by Pérez-Invernón et al. (2022) in the Ebro Valley and the Pyrenees by using the TROP-DLR products. As previously reported by Allen, Pickering, Bucselá, et al. (2021); Pérez-Invernón et al. (2022), negative values of tropospheric  $\text{NO}_x$  indicate that the average stratospheric column exceeds the local vertical column or that the tropospheric background exceeds the signal. The remarkably low average ages of the flashes on 12 August 2018 and 23 August 2018 suggest that lightning activity had just begun to increase at the time of the TROPOMI overpass. As a consequence, the OCP values were low (Bucselá et al., 2019) and the measured SCD of  $\text{NO}_2$  were lower than in other cases. It is important to remark that the effect of cloud opacity is introduced in the calculation of the VCD tropospheric  $\text{LNO}_x$  by the calculation of the  $\text{AMFLNO}_x$ .

### 3.2. $\text{LNO}_x$ Estimate for Each Thunderstorm

The obtained mean flash length,  $\text{LNO}_x$  PE per flash and  $\text{LNO}_x$  PE per channel length are shown in Table 1, together with an estimation of their variability by using the standard deviation calculated between the 16 studied cases. In addition, the column 3 shows the mean flash frequency calculated during 1 hr centered at the mean age of the flashes. The median and the mean flash length ranges between 5 and 47 km and between 11 and 107 km, respectively. The distribution of channel lengths and total number of flashes for each case are plotted in Figures 1a and 1b, respectively. Figure 1a shows that the values of the channel lengths follow a log-normal distribution. Interestingly, there is an inverse relationship between flash rate and flash size (Figure 1b), as reported previously by Bruning and MacGorman (2013). The  $\text{LNO}_x$  PE per flash by using the 10th and the 30th background- $\text{NO}_x$  methods are  $108 \pm 82$  mol  $\text{NO}_x/\text{f}$  and  $54 \pm 42$  mol  $\text{NO}_x/\text{f}$ , respectively. These values are similar to the values reported by Pérez-Invernón et al. (2022). In turn, the obtained  $\text{LNO}_x$  PE per flash length, calculated as the  $\text{LNO}_x$  PE per flash divided by the mean flash length for each case, are  $1.6 \pm 1.0 \times 10^{21}$  molec  $\text{NO}_x/\text{m}$  and  $0.8 \pm 0.5 \times 10^{21}$  molec  $\text{NO}_x/\text{m}$  when using the 10th and the 30th background- $\text{NO}_x$  methods, respectively. The  $\text{LNO}_x$  PE per flash length, which falls within the range of 0.3–2.6 molec  $\text{NO}_x/\text{m}$ , closely aligns with the results obtained in laboratory experiments by Wang et al. (1998) ( $1.4\text{--}5.2 \times 10^{21}$  molec ( $\text{NO}_x/\text{m}$ )), and from airborne measurements by Stith et al. (1999) in Colorado ( $0.2\text{--}10 \times 10^{21}$  molec ( $\text{NO}_x/\text{m}$ )), by Huntrieser et al. (2002) in Germany ( $0.07\text{--}10 \times 10^{21}$  molec ( $\text{NO}_x/\text{m}$ )), and by Skamarock et al. (2003) in Colorado ( $1 \times 10^{21}$  molec ( $\text{NO}_x/\text{m}$ )). However, the obtained mean  $\text{LNO}_x$  PE per flash length is slightly below the values reported by other airborne

**Table 1**

Results for the 16 Studied Cases Using the TROP-DLR Products and Lightning Measurements in the Region 38.4–42.5N/1.2W–3E and Using the 10th and the 30th Percentile of the  $V_{tropNO_x}$  Over Non-Flashing Pixels With Deep Convection to Estimate  $V_{tropbk}$

Case	F	F	Mean	Mean/median	LNO <sub>x</sub> PE	LNO <sub>x</sub> PE	Mean/median	Mean/median
	ENGLN	ELMA	Flash Frequency	Flash Length	$V_{tropbk}$ 10th	$V_{tropbk}$ 30th	LNO <sub>x</sub> PE $V_{tropbk}$ 10th	LNO <sub>x</sub> PE $V_{tropbk}$ 30th
	(N flashes)	(N flashes)	(F/h)	(km)	(mol NO <sub>x</sub> /f)	(mol NO <sub>x</sub> /f)	(×10 <sup>21</sup> molec NO <sub>x</sub> /m)	(×10 <sup>21</sup> molec NO <sub>x</sub> /m)
9 August 2018	28,523	20,483	12,747	27/11	39	30	0.9/2.1	0.7/1.6
12 August 2018	2,904	471	2,490	15/9	9	3	0.4/0.6	0.1/0.2
17 August 2018	39,452	4,030	7,565	24/9	75	55	1.9/5.0	1.4/3.7
23 August 2018	650	676	355	29/15	130	91	2.7/5.2	1.9/3.7
3 September 2018	7,473	6,057	2,623	70/25	36	13	0.3/0.9	0.1/0.3
5 September 2018	10,183	5,452	3,474	16/6	46	19	1.7/4.6	0.7/1.9
6 September 2018	16,673	1,816	3,629	11/5	19	9	1.0/2.3	0.5/1.1
15 September 2018	6,610	3,804	1,196	75/32	180	81	1.4/3.4	0.7/1.5
14 October 2018	3,149	219	1,734	35/23	118	53	2.0/3.1	0.9/1.4
19 October 2018	5,339	4,321	1,238	107/47	161	85	0.9/2.1	0.5/1.1
15 November 2018	3,688	1,094	814	76/18	161	75	1.3/5.4	0.6/2.5
26 July 2019	1,639	428	385	51/27	132	66	1.6/2.9	0.8/1.5
21 September 2019	12,845	3,710	1,720	18/6	25	6	0.8/2.5	0.2/0.6
22 October 2019	33,540	2,591 (*)	8,574	35/15	68	33	1.2/2.7	0.6/1.3
21 January 2020	5,126	432	1,171	65/45	316	166	2.9/4.2	1.5/2.2
10 August 2020	2,414	971	260	32/21	216	86	4.1/6.2	1.6/2.5
Mean ± σ					108 ± 82	54 ± 42	1.6 ± 1.0/3.3 ± 1.6	0.8 ± 0.5/1.7 ± 1.0

Note. (\*): ELMA was not in operation before 11:30 hr on 22 October 2019, causing that older flashes are missing).

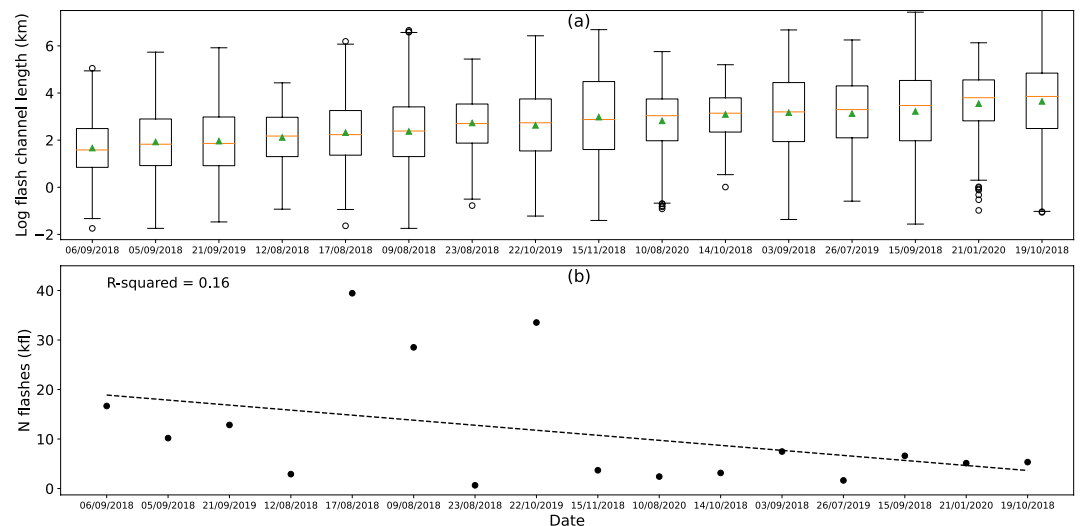


**Figure 1.** (a): Box plots showing the distribution of channel lengths for each of the 16 thunderstorm cases investigated. The green triangles show the mean flash lengths. The orange line indicates the median flash length. Black circles indicate outliers. The cases are sorted by increasing median values. (b): Total number of flashes 5 hr before the overpass of TROPOMI (N flashes) for each of the cases. We have included a linear regression (dashed line) and the R-squared coefficient of the regression model.

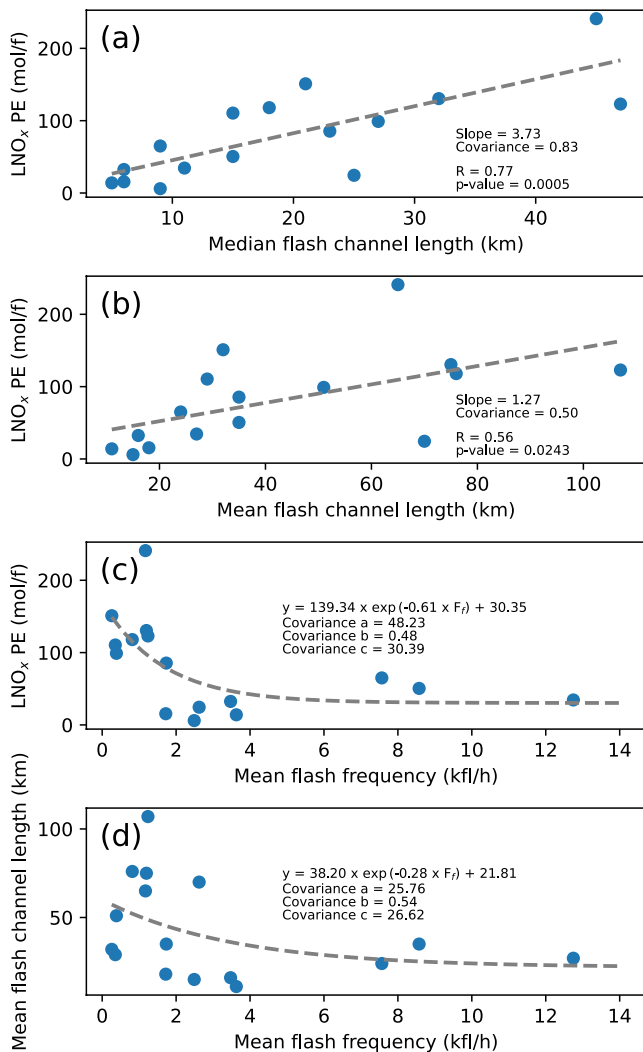


**Figure 2.**  $LNO_x$  PE versus the median (a) and the mean (b) flash channel length,  $LNO_x$  PE versus the mean flash frequency (c) and mean flash channel length (d) versus mean flash frequency for 16 cases. We have included the linear regression (dashed line), the Pearson correlation coefficient ( $R$ ) and the corresponding  $p$ -value in panels (a), (b), as well as a fit to an exponential decay in panels (c), (d).

### 3.4. Discussion

The obtained positive relationship between the  $LNO_x$  PE per flash and the flash channel length is influenced by the vertical structure of lightning flashes, that is, how the branches of the flash are distributed at different altitudes as a function of the total flash length. As shown in Figure 3a, the vertical distribution of lightning flashes below a given total length (colored lines) and the  $LNO_x$  mass distribution (dashed line), which is introduced in the EMAC simulation to calculate the AMFL $LNO_x$ , exhibit some interesting features. The layer with the highest proportion of the total lightning channel is located at an altitude of 10 km. However, for longer lightning flashes, the channel occupies a greater horizontal area at lower altitudes. This is more clearly observed in Figure 3b, which shows the percentage of the lightning channel above 10 km altitude depending on the total flash channel length. Thus, longer flashes could release more  $LNO_x$  at lower altitudes than shorter flashes. Additionally, low

measurements in Germany (see Schumann and Huntrieser (2007) for more comparisons) and in rocket-triggered lightning ( $2.0 \times 10^{22}$ – $2.4 \times 10^{22}$  molecules  $NO_x$   $m^{-1}$ ) (Rahman et al., 2007).

### 3.3. $LNO_x$ PE Estimate and Flash Channel Length

We examine the correlation between the  $LNO_x$  PE estimate and the flash length reported by ELMA. We used the  $LNO_x$  PE estimate averaged by considering the 30th and the 10th percentile of the vertical column density of tropospheric  $NO_x$  ( $V_{tropNO_x}$ ) to estimate the vertical column density of background  $NO_x$  ( $V_{tropbck}$ ) (columns 6 and 9 in Table 1). The results by considering separately the 30th and the 10th percentile of the vertical column density of tropospheric  $NO_x$  ( $V_{tropNO_x}$ ) to estimate the vertical column density of background  $NO_x$  are plotted in Figure S34 in Supporting Information S1 and confirm the conclusions from Figure 2. We plot in Figures 2a and 2b the  $LNO_x$  PE estimate versus the median and the mean flash channel length for the 16 studied thunderstorms, respectively. We calculated the Pearson correlation coefficient ( $R$ ) between the  $LNO_x$  PE and the median and mean flash channel length, obtaining  $R = 0.77$  and  $R = 0.56$  and  $p$ -values of 0.0005 and 0.0243, respectively. Figure S35 in Supporting Information S1 exhibits the plot identical to that of Figure 2, but with the  $y$ -axis shown on a logarithmic scale.

Figure 2c displays the  $LNO_x$  PE versus the mean flash frequency, while Figure 2d shows the mean flash channel length versus mean flash frequency. In turn, we have fitted the dependence of  $LNO_x$  PE (in mol  $NO_x$  per flash) on lightning frequency and the mean flash channel length versus the mean flash frequency using exponential decays according to

$$LNO_x PE = a \times \exp(-b \times F_f) + c, \quad (1)$$

and

$$Mean \ flash \ length = a' \times \exp(-b' \times F_f) + c', \quad (2)$$

respectively, where  $F_f$  is the mean flash frequency in units of kfl/h and the coefficients of the fitting are  $a = 139.34$ ,  $b = 0.61$  and  $c = 30.35$  and  $a' = 38.20$ ,  $b' = 0.28$  and  $c' = 21.81$ , respectively. Figures 2c and 2d also indicate the covariance of the fitting coefficients, indicating the goodness of the fit. Despite the low total number of thunderstorms analyzed in comparison with Bucselá et al. (2019), the obtained results are consistent with Bucselá et al. (2019, Figure 11c). These results indicate that thunderstorms with higher flash frequency produce shorter lightning channels and a lower amount of  $LNO_x$  per flash.

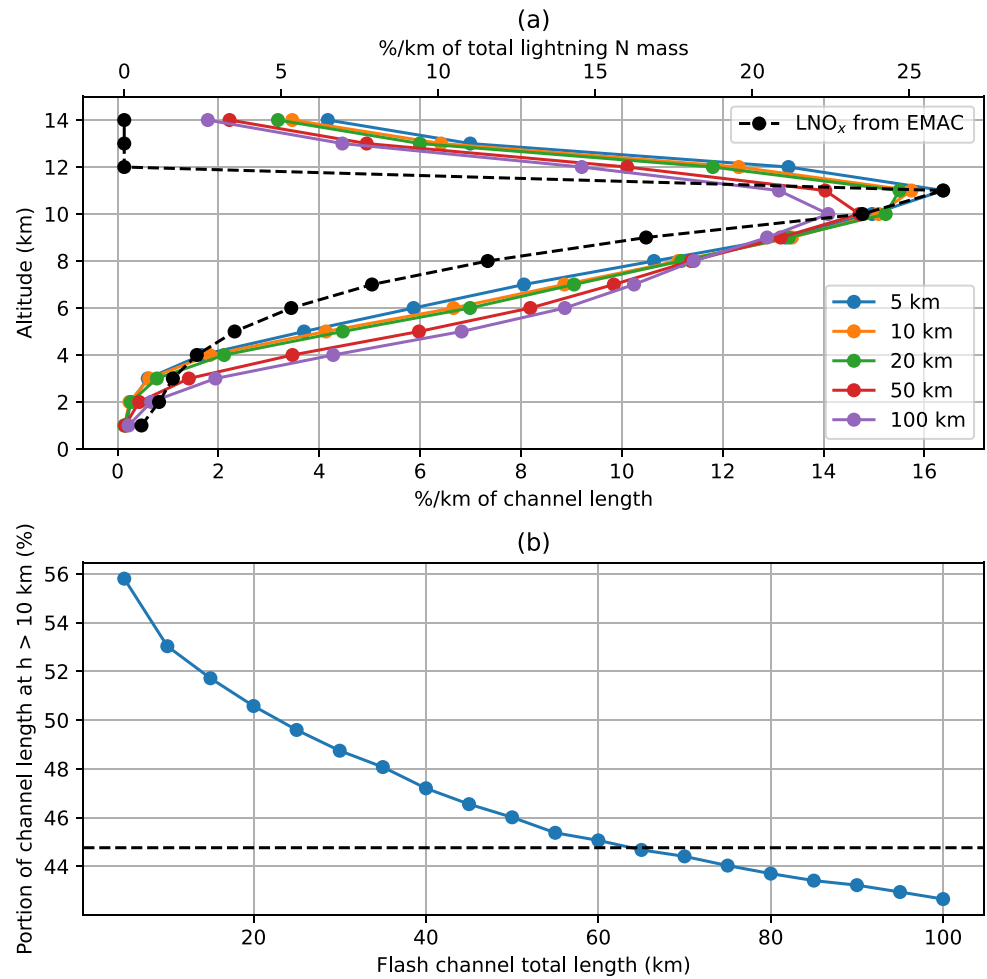


**Figure 3.** (a): Vertical distribution of lightning flashes below a given total length (colored lines) and LNO<sub>x</sub> mass distribution (dashed line), which is introduced in the EMAC simulation to calculate the AMFLNO<sub>x</sub> factors. (b): Percentage of the lightning channel above 10 km altitude depending on the total flash channel length. These profiles have been calculated from the mean profiles of 16 cases.

altitude flashes are more likely to produce cloud-to-ground flashes. Extensive stratiform flashes usually produce positive CG flashes that can trigger sprites (e.g., van der Velde et al. (2014)) and its associated currents and faster leaders (typically at 5–8 km altitude) may produce more NO<sub>x</sub>. However, the EMAC simulation used to extract the a priori LNO<sub>x</sub> vertical profile for calculating the AMFLNO<sub>x</sub> factors (dashed lines in Figures 3a and 3b) does not account for variations in the LNO<sub>x</sub> profile with lightning channel length. The AMFLNO<sub>x</sub> factors are then used to estimate the VCD of LNO<sub>x</sub> from the reported SCD of NO<sub>2</sub> in the upper atmosphere. Consequently, shorter lightning flashes could inject a higher proportion of LNO<sub>x</sub> into the upper atmosphere compared to longer flashes. Therefore, the a priori profiles used to estimate the AMFLNO<sub>x</sub> factors may overestimate the LNO<sub>x</sub> in the lower atmosphere and, consequently, the LNO<sub>x</sub> PE per channel length for shorter lightning flashes. In particular, Figure 3b suggests that the imposed LNO<sub>x</sub> mass vertical profile could overestimate the LNO<sub>x</sub> per flash for lightning flashes with a total channel length below 65 km, which represents the 91% of the flashes detected by ELMA in this study. To reduce this limitation, simulations using a cloud-resolved atmospheric model with an adaptive vertical profile of the LNO<sub>x</sub> mass would be needed.

Another contributing factor to the overestimation of LNO<sub>x</sub> produced by shorter lightning flashes is the low OCP typically associated with these flashes. Since shorter lightning flashes tend to occur in thunderstorms with high flash frequencies, they may tend to occur in pixels with lower OCP values. Pixels with lower OCP have larger portion of the atmosphere below clouds where NO<sub>2</sub> is invisible to TROPOMI. As a consequence, low SCD of NO<sub>2</sub> are reported by TROPOMI (see Figures S1 and S4 in Supporting Information S1). This means that the VCD



$LNO_x$  estimate is more influenced by the calculated  $AMFLNO_x$ , which can exacerbate the overestimation of  $LNO_x$  PE per flash for shorter lightning flashes.

The EMAC  $LNO_x$  profile plays a crucial role in influencing the calculation of the VCD  $LNO_x$  due to its direct impact on the determination of  $AMF_{LNO_x}$ . Both background- $NO_x$  and  $LNO_x$  calculations are dependent on the VCD  $LNO_x$ , which means that the EMAC  $LNO_x$  profiles can have an effect on the estimation of background- $NO_x$ . However, it is important to note that the primary factor influencing background- $NO_x$  is the difference in VCD  $NO_x$  between pixels with and without flashes, as highlighted in Pérez-Invernón et al. (2022).

#### 4. Conclusions

Estimates of lightning produced  $NO_x$  ( $LNO_x$ ) Production Efficiency (PE) by different methods suggest a high variability of  $LNO_x$  PE and flash characteristics. The use of a Lightning Mapping Array (LMA) has proven to be a powerful tool to estimate some flash characteristics, such as the flash length. We have combined the TROP-Ospheric Monitoring Instrument (TROPOMI) Deutsches Zentrum für Luft- und Raumfahrt (DLR) TROP-DLR operational cloud and  $NO_2$  research products with lightning measurements from the Ebro LMA (ELMA) to investigate the relationship between  $LNO_x$  PE, flash rate and flash length using 16 thunderstorm cases observed over the eastern coast of the Iberian Peninsula. To the best of our knowledge, the results presented in this work are the first satellite-based study to demonstrate that  $LNO_x$  per flash is proportional to flash length by using LMA-based estimates of  $LNO_x$  and, in turn, the first that employs LMA measurements to estimate  $LNO_x$  in Europe. Our results demonstrate that the combination of satellite-based retrievals of  $NO_2$  with LMA systems is an innovative and promising approach to understand the variability in the production of  $LNO_x$  per flash in active thunderstorms. The main conclusions of this work are:

1. TROP-DLR retrieval of  $NO_2$  together with LMA lightning measurements are useful to investigate the relationships between the production of  $LNO_x$  per flash and the flash characteristics.
2. TROP-DLR data suggest an inverse relationship between  $LNO_x$  PE and flash rate, previously found by Bucseła et al. (2019); Allen et al. (2019); Allen, Pickering, Bucseła, et al. (2021) and, in turn, a positive relationship between  $LNO_x$  PE and flash length.
3. Space-based observations of mean  $LNO_x$  per flash length obtained in this work vary between  $0.3 \times 10^{21}$  molec  $NO_x/m$  and  $2.6 \times 10^{21}$  molec  $NO_x/m$  and fall at the lower end of the range of previous estimations (Beirle et al., 2004; Pickering et al., 2016; Rahman et al., 2007; Schumann & Huntrieser, 2007; Stith et al., 1999; Wang et al., 1998). In turn, the mean  $LNO_x$  PE per flash estimate ranges between 42 mol  $NO_x/f$  and 108 mol  $NO_x/f$ .

The Meteosat Third Generation (MTG) Imaging (launched in Dec 2022) and Sounding (expected by Q3 2024) satellites (Holmlund et al., 2021) will notably contribute to reduce the uncertainty in the  $LNO_x$  estimates over Europe. The MTG Lightning Imager (LI) (Dobber & Grandell, 2014) reports the occurrence of total lightning flashes from space every 1 ms, complementing the lightning data provided by ground-based lightning networks. More significantly, the MTG high-resolution Sentinel-4 (or Ultraviolet-Visible-Near-Infrared UVN) sounder will provide for the first time continuous (1-hourly)  $NO_2$  estimates from space over Europe. The  $NO_2$  measurements of MTG-UVN will enable us to calculate the temporal evolution of the  $LNO_x$  PE over particular thunderstorms during long-lived mesoscale convective systems (MCS) and will be useful to estimate the background- $NO_x$  before the inception of lightning.

#### Data Availability Statement

The official TROPOMI data are available via ESA's public data hub after registration (<https://s5phub.copernicus.eu/dhus>, last access: 25 May 2023). The ERA5 meteorological data are freely accessible through the global climate from the Copernicus Climate Change Service Climate Data Store (Hersbach et al., 2023). ELMA lightning data are available from UPC Lightning Research Group (<https://elma.upc.edu>, last access: 25 May 2023) by e-mail to a member of the group (<https://elma.upc.edu/contacto>, last access: 15 Sep 2023). ENGLN lightning data are available upon request from Earth Networks (<https://www.earthnetworks.com>, last access: 25 May 2023) by e-mail to [info@earthnetworks.com](mailto:info@earthnetworks.com).

**Acknowledgments**

The project that gave rise to these results received the support of a fellowship from “la Caixa” Foundation (ID 100010434). The fellowship code is LCF/BQ/PI22/11910026 (F.J.P.I.). Additionally, this work was supported by grants PID2019-109269RB-C43 (F.J.P.I. and F.J.G.V.), PID2022-136348NB-C31 (F.J.P.I. and F.J.G.V.) and PID2019-109269RB-C42 (O.V.W., J.M. and J.L.) funded by MCIN/AEI/10.13039/501100011033 and “ERDF A way of making Europe.” F.J.P.I. and F.J.G.V. acknowledge financial support from the grant CEX2021-001131-S funded by MCIN/AEI/10.13039/501100011033.

**References**

Allen, D. J., Pickering, K. E., Bucselá, E., Krotkov, N., & Holzworth, R. (2019). Lightning NO<sub>x</sub> production in the tropics as determined using OMI NO<sub>2</sub> retrievals and WWLLN stroke data. *Journal of Geophysical Research: Atmospheres*, *124*(23), 13498–13518. <https://doi.org/10.1029/2019JD030561>

Allen, D. J., Pickering, K. E., Bucselá, E., Van Geffen, J., Lapierre, J., Koshak, W., & Eskes, H. (2021). Observations of lightning NO<sub>x</sub> production from Tropospheric Monitoring Instrument case studies over the United States. *Journal of Geophysical Research: Atmospheres*, *126*(10), e2020JD034174. <https://doi.org/10.1029/2020JD034174>

Allen, D. J., Pickering, K. E., Lamsal, L., Mach, D. M., Quick, M. G., Lapierre, J., et al. (2021). Observations of lightning NO<sub>x</sub> production from GOES-R post launch test field campaign flights. *Journal of Geophysical Research: Atmospheres*, *126*(8), e2020JD033769. <https://doi.org/10.1029/2020JD033769>

Beirle, S., Platt, U., Wenig, M., & Wagner, T. (2004). NO<sub>x</sub> production by lightning estimated with GOME. *Advances in Space Research*, *34*(4), 793–797. <https://doi.org/10.1016/j.asr.2003.07.069>

Bruning, E. C., & MacGorman, D. R. (2013). Theory and observations of controls on lightning flash size spectra. *Journal of the Atmospheric Sciences*, *70*(12), 4012–4029. <https://doi.org/10.1175/JAS-D-12-0289.1>

Bruning, E. C., & Thomas, R. J. (2015). Lightning channel length and flash energy determined from moments of the flash area distribution. *Journal of Geophysical Research: Atmospheres*, *120*(17), 8925–8940. <https://doi.org/10.1002/2015JD023766>

Bucselá, E. J., Pickering, K. E., Allen, D. J., Holzworth, R. H., & Krotkov, N. A. (2019). Midlatitude lightning NO<sub>x</sub> production efficiency inferred from OMI and WWLLN data. *Journal of Geophysical Research: Atmospheres*, *124*(23), 13475–13497. <https://doi.org/10.1029/2018JD029824>

Dobber, M., & Grandell, J. (2014). Meteosat Third Generation (MTG) Lightning Imager (LI) instrument performance and calibration from user perspective.

Gordillo-Vázquez, F. J., Pérez-Invernón, F. J., Huntrieser, H., & Smith, A. K. (2019). Comparison of six lightning parameterizations in CAM5 and the impact on global atmospheric chemistry. *Earth and Space Science*, *6*(12), 2317–2346. <https://doi.org/10.1029/2019EA000873>

Hansen, A. E., Fuelberg, H. E., & Pickering, K. E. (2010). Vertical distributions of lightning sources and flashes over Kennedy Space Center, Florida. *Journal of Geophysical Research*, *115*(D14). <https://doi.org/10.1029/2009JD013143>

Hersbach, H., Bell, B., Berrisford, P., Biavati, G., Horányi, A., Muñoz Sabater, J., et al. (2023). ERA5 hourly data on pressure levels from 1940 to present [Dataset]. Copernicus Climate Change Service (C3S) Climate Data Store (CDS). <https://doi.org/10.24381/cds.bd0915c6>

Hersbach, H., Bell, B., Berrisford, P., Hirahara, S., Horányi, A., Muñoz-Sabater, J., et al. (2020). The ERA5 global reanalysis. *Quarterly Journal of the Royal Meteorological Society*, *146*(730), 1999–2049. <https://doi.org/10.1002/qj.3803>

Holmlund, K., Grandell, J., Schmetz, J., Stuhlmann, R., Bojkov, B., Munro, R., et al. (2021). Meteosat Third Generation (MTG): Continuation and innovation of observations from geostationary orbit. *Bulletin of the American Meteorological Society*, *102*(5), E990–E1015. <https://doi.org/10.1175/BAMS-D-19-0304.1>

Huntrieser, H., Feigl, C., Schlager, H., Schröder, F., Gerbig, C., Van Velthoven, P., et al. (2002). Airborne measurements of NO<sub>x</sub>, tracer species, and small particles during the European Lightning Nitrogen Oxides Experiment. *Journal of Geophysical Research*, *107*(D11), ACH5-1–ACH5-24. <https://doi.org/10.1029/2000JD000209>

Huntrieser, H., Schlager, H., Roiger, A., Lichtenstern, M., Schumann, U., Kurz, C., et al. (2007). Lightning-produced NO<sub>x</sub> over Brazil during TROCCINOX: Airborne measurements in tropical and subtropical thunderstorms and the importance of mesoscale convective systems. *Atmospheric Chemistry and Physics*, *7*(11), 2987–3013. <https://doi.org/10.5194/acp-7-2987-2007>

Huntrieser, H., Schumann, U., Schlager, H., Höller, H., Giez, A., Betz, H.-D., et al. (2008). Lightning activity in Brazilian thunderstorms during TROCCINOX: Implications for NO<sub>x</sub> production. *Atmospheric Chemistry and Physics*, *8*(4), 921–953. <https://doi.org/10.5194/acp-8-921-2008>

Jöckel, P., Tost, H., Pozzer, A., Kunze, K., Kirner, O., Brenninkmeijer, C. A., et al. (2016). Earth system chemistry integrated modelling (ESCiMo) with the modular earth submodel system (MESSy) version 2.51. *Geoscientific Model Development*, *9*(3), 1153–1200. <https://doi.org/10.5194/gmd-9-1153-2016>

Koshak, W., Peterson, H., Biazar, A., Khan, M., & Wang, L. (2014). The NASA lightning nitrogen oxides model (LNOM): Application to air quality modeling. *Atmospheric Research*, *135*, 363–369. <https://doi.org/10.1016/j.atmosres.2012.12.015>

Lapierre, J. L., Laughner, J. L., Geddes, J. A., Koshak, W. J., Cohen, R. C., & Pusede, S. E. (2020). Observing US regional variability in lightning NO<sub>2</sub> production rates. *Journal of Geophysical Research: Atmospheres*, *125*(5), e2019JD031362. <https://doi.org/10.1029/2019JD031362>

Liu, S., Valks, P., Pinaridi, G., Xu, J., Chan, K. L., Argyrouli, A., et al. (2021). An improved tropospheric NO<sub>2</sub> column retrieval algorithm for TROPOMI over Europe. *Atmospheric Measurement Techniques*, *1–43*. <https://doi.org/10.5194/amt-2021-39>

López, J. A., Pineda, N., Montanyà, J., van der Velde, O., Fabró, F., & Romero, D. (2017). Spatio-temporal dimension of lightning flashes based on three-dimensional lightning mapping array. *Atmospheric Research*, *197*, 255–264. <https://doi.org/10.1016/j.atmosres.2017.06.030>

Loyola, D. G., Gimeno García, S., Lutz, R., Argyrouli, A., Romahn, F., Spurr, R. J., et al. (2018). The operational cloud retrieval algorithms from TROPOMI on board Sentinel-5 precursor. *Atmospheric Measurement Techniques*, *11*(1), 409–427. <https://doi.org/10.5194/amt-11-409-2018>

Mecikalski, R. M., & Carey, L. D. (2018). Radar reflectivity and altitude distributions of lightning as a function of IC, CG, and HY flashes: Implications for LNO<sub>x</sub> production. *Journal of Geophysical Research: Atmospheres*, *123*(22), 12–796. <https://doi.org/10.1029/2018JD029263>

Nault, B. A., Laughner, J. L., Wooldridge, P. J., Crouse, J. D., Dibb, J., Diskin, G., et al. (2017). Lightning NO<sub>x</sub> emissions: Reconciling measured and modeled estimates with updated NO<sub>x</sub> chemistry. *Geophysical Research Letters*, *44*(18), 9479–9488. <https://doi.org/10.1002/2017GL074436>

Pérez-Invernón, F. J., Huntrieser, H., Erbertseder, T., Loyola, D., Valks, P., Liu, S., et al. (2022). Quantification of lightning-produced NO<sub>x</sub> over the Pyrenees and the Ebro Valley by using different TROPOMI-NO<sub>2</sub> and cloud research products. *Atmospheric Measurement Techniques*, *15*(11), 3329–3351. <https://doi.org/10.5194/amt-2021-286>

Petetin, H., Guevara, M., Compennolle, S., Bowdalo, D., Bretonnière, P.-A., Enciso, S., et al. (2023). Potential of TROPOMI for understanding spatio-temporal variations in surface NO<sub>2</sub> and their dependencies upon land use over the Iberian Peninsula. *Atmospheric Chemistry and Physics*, *23*(7), 3905–3935. <https://doi.org/10.5194/acp-23-3905-2023>

Pickering, K. E., Bucselá, E., Allen, D., Ring, A., Holzworth, R., & Krotkov, N. (2016). Estimates of lightning NO<sub>x</sub> production based on OMI NO<sub>2</sub> observations over the gulf of Mexico. *Journal of Geophysical Research: Atmospheres*, *121*(14), 8668–8691. <https://doi.org/10.1002/2015JD024179>

Pineda, N., Esteban, P., Trapero, L., Soler, X., & Beck, C. (2010). Circulation types related to lightning activity over Catalonia and the Principality of Andorra. *Physics and Chemistry of the Earth, Parts A/B/C*, *35*(9), 469–476. (Classifications of Atmospheric Circulation Patterns – Theory and Applications). <https://doi.org/10.1016/j.pce.2009.12.009>

Pineda, N., Rigo, T., Montanyà, J., & van der Velde, O. A. (2016). Charge structure analysis of a severe hailstorm with predominantly positive cloud-to-ground lightning. *Atmospheric Research*, *178*, 31–44. <https://doi.org/10.1016/j.atmosres.2016.03.010>

- Rahman, M., Cooray, V., Rakov, V. A., Uman, M., Liyanage, P., DeCarlo, B., et al. (2007). Measurements of  $\text{NO}_x$  produced by rocket-triggered lightning. *Geophysical Research Letters*, *34*(3), L03816. <https://doi.org/10.1029/2006GL027956>
- Rison, W., Thomas, R. J., Krehbiel, P. R., Hamlin, T., & Harlin, J. (1999). A GPS-based three-dimensional lightning mapping system: Initial observations in central New Mexico. *Geophysical Research Letters*, *26*(23), 3573–3576. <https://doi.org/10.1029/1999GL010856>
- Schumann, U., & Huntrieser, H. (2007). The global lightning-induced nitrogen oxides source. *Atmospheric Chemistry and Physics*, *7*(14), 3823–3907. <https://doi.org/10.5194/acp-7-3823-2007>
- Skamarock, W. C., Dye, J. E., Defer, E., Barth, M., Stith, J. L., Ridley, B. A., & Baumann, K. (2003). Observational-and modeling-based budget of lightning-produced  $\text{NO}_x$  in a continental thunderstorm. *Journal of Geophysical Research*, *108*(D10). <https://doi.org/10.1029/2002jd002163>
- Stark, M., Harrison, J., & Anastasi, C. (1996). Formation of nitrogen oxides by electrical discharges and implications for atmospheric lightning. *Journal of Geophysical Research*, *101*(D3), 6963–6969. <https://doi.org/10.1029/95JD03008>
- Stith, J., Dye, J., Ridley, B., Laroche, P., Defer, E., Baumann, K., et al. (1999).  $\text{NO}$  signatures from lightning flashes. *Journal of Geophysical Research*, *104*(D13), 16081–16089. <https://doi.org/10.1029/1999JD900174>
- van der Velde, O. A., & Montanyà, J. (2013). Asymmetries in bidirectional leader development of lightning flashes. *Journal of Geophysical Research: Atmospheres*, *118*(24), 13–504. <https://doi.org/10.1002/2013JD020257>
- van der Velde, O. A., Montanyà, J., Soula, S., Pineda, N., & Mlynarczyk, J. (2014). Bidirectional leader development in sprite-producing positive cloud-to-ground flashes: Origins and characteristics of positive and negative leaders. *Journal of Geophysical Research: Atmospheres*, *119*(22), 12–755. <https://doi.org/10.1002/2013JD021291>
- Van Geffen, J., Eskes, H., Compennolle, S., Pinaridi, G., Verhoelst, T., Lambert, J.-C., et al. (2022). Sentinel-5P TROPOMI  $\text{NO}_2$  retrieval: Impact of version v2.2 improvements and comparisons with OMI and ground-based data. *Atmospheric Measurement Techniques*, *15*(7), 2037–2060. <https://doi.org/10.5194/amt-15-2037-2022>
- Veeffkind, J., Aben, I., McMullan, K., Förster, H., De Vries, J., Otter, G., et al. (2012). TROPOMI on the ESA sentinel-5 precursor: A GMES mission for global observations of the atmospheric composition for climate, air quality and ozone layer applications. *Remote Sensing of Environment*, *120*, 70–83. <https://doi.org/10.1016/j.rse.2011.09.027>
- Wang, Y., DeSilva, A., Goldenbaum, G., & Dickerson, R. (1998). Nitric oxide production by simulated lightning: Dependence on current, energy, and pressure. *Journal of Geophysical Research*, *103*(D15), 19149–19159. <https://doi.org/10.1029/98JD01356>
- Zeldovich, Y., Frank-Kamenetskii, D., & Sadovnikov, P. (1947). *Oxidation of nitrogen in combustion*. Publishing House of the Acad of Sciences of USSR.
- Zhang, X., Yin, Y., van der A, R., Eskes, H., van Geffen, J., Li, Y., et al. (2022). Influence of convection on the upper-tropospheric  $\text{O}_3$  and  $\text{NO}_x$  budget in southeastern China. *Atmospheric Chemistry and Physics*, *22*(9), 5925–5942. <https://doi.org/10.5194/acp-22-5925-2022>
- Zhu, Y., Rakov, V., Tran, M., Stock, M., Heckman, S., Liu, C., et al. (2017). Evaluation of ENTLN performance characteristics based on the ground truth natural and rocket-triggered lightning data acquired in Florida. *Journal of Geophysical Research: Atmospheres*, *122*(18), 9858–9866. <https://doi.org/10.1002/2017jd027270>